Response to reviewer#1

Thank you for your careful works and valuable comments. The comments and suggestions are very useful for our manuscript. We have carefully studied these comments and suggestions and made some changes in our manuscript.

Comment 1)

Measurements of the vertical fluxes of species, heat, and horizontal momentum are rare so new measurements of the Na and heat fluxes are an important contribution to our knowledge wave-induced transport. Although the authors claim in the Abstract to present seasonal variations of Na and heat fluxes, they only presented what I think are annual mean profiles (Figs. 11 & 12). Furthermore, although their powerful lidar (PA=1.2 Wm2, Δz=61.44 m, Δt=1 min) should be capable of measuring vertical fluxes at high temporal resolution, the data were smoothed to resolutions of Δz=2 km and Δt=30 min, before the computing the vertical fluxes. This is a significant problem, at least for the heat flux, where Guo & Liu (2021) have shown that most of the heat transport is induced by waves with periods less than 1 h, waves which were eliminated from the Hainan dataset by their smoothing procedure. At the very least, the authors need to reprocess their flux data (both heat and Na fluxes) with a temporal resolution of 2.5 or 3 min so that waves with periods of 5-6 min or longer are included. In addition, the authors need to present the seasonal profiles of the Na and heat fluxes as they claimed in the Abstract.

Response:

Thank you for your comment. We reprocessed the lidar data using a 3-minute temporal resolution and applied smoothing with a 2 km Hamming window. Data products were then filtered based on the following uncertainty thresholds: sodium density <3%, temperature <5 K, and vertical wind <3 m s^{-1}. Using this quality-controlled dataset, we recalculated the annual mean flux results.

As shown in Figure 1, the result of heat flux is slightly different from that in Figure 11 of our manuscript. The peaks at 89km and 84km still exist, but the absolute value

increases by approximately 0.4 K m s^{-1}. There is also a small peak at about 95km. The entire heat flux reaches the peak at about -1.4 K m s^{-1} at 92km, and the corresponding heating rate is also slightly different. But in Hefei, China, Li et al (2022) had shown that the heat flux in the mesopause region is contributed primarily by the long-period (more than 1 hr) GWs. This might be because the temperature spectrum varies with w^{-2}, implying that long-period GWs dominate temperature perturbations.

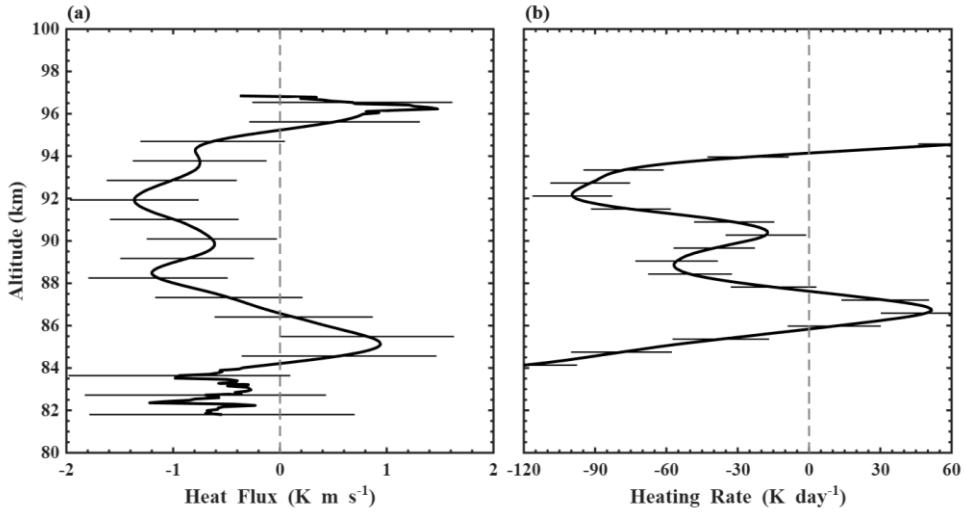

Figure 1. The vertical flux of sensible heat. (a) Annual mean sensible heat flux derived from vertical wind and temperature measurements at Hainan, China, and (b) the corresponding heating rates. Error bars are shown as thin lines.

The sodium flux is shown in Figure 2. The peak at 88km still exists, but the value drops from 50 m s^{-1}·cm^{-3} to 25 m s^{-1}·cm^{-3}. Meanwhile, the overall peak rises to 93km, with a value of -65 m s^{-1}·cm^{-3}. The corresponding sodium production rate is between 89 and 94km. More details are available.

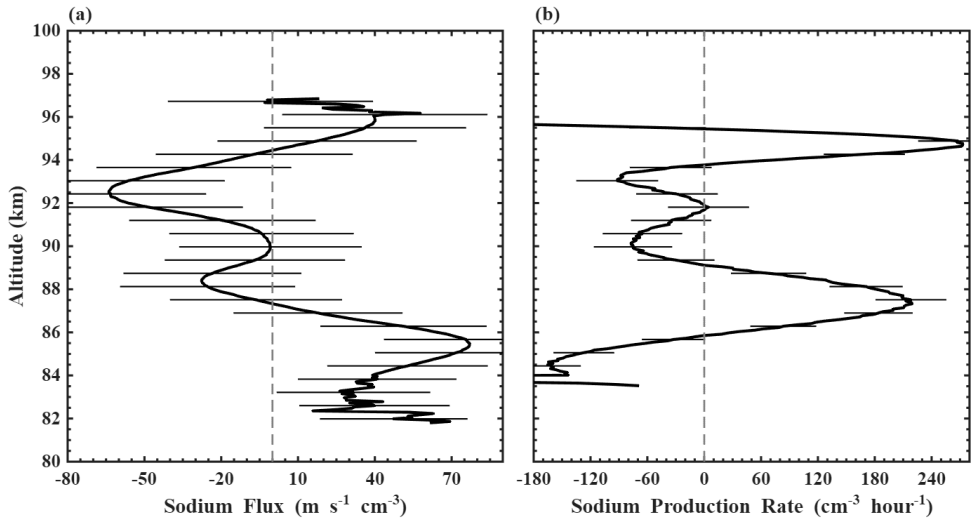

Figure 2. The dynamical flux of sodium. (a) Na flux due to dissipating gravity waves calculated from the measured Na density and vertical wind measurements at Hainan. (b) Na production rate calculated from measured Na flux at Hainan. Error bars are shown as thin lines.

Figure 3a presents the seasonal variation in vertical heat flux. The fluxes in all four seasons generally align with the annual mean, with winter contributing the most, consistent with the observational distribution shown in Figure 8. Notably, a conspicuous negative anomaly at ~85 km in autumn also corresponds to a feature in the annual average. Similarly, the seasonal sodium flux in Figure 3b shows winter as the dominant contributor. Negative anomalies at 86 km in summer and 91 km in autumn are also reflected in the annual mean profile. Compared with winter, the observational data for our spring, summer and autumn seasons are all scarce. Therefore, the manuscript mainly presents the annual average of fluxes and does not discuss the influence of seasonal changes.

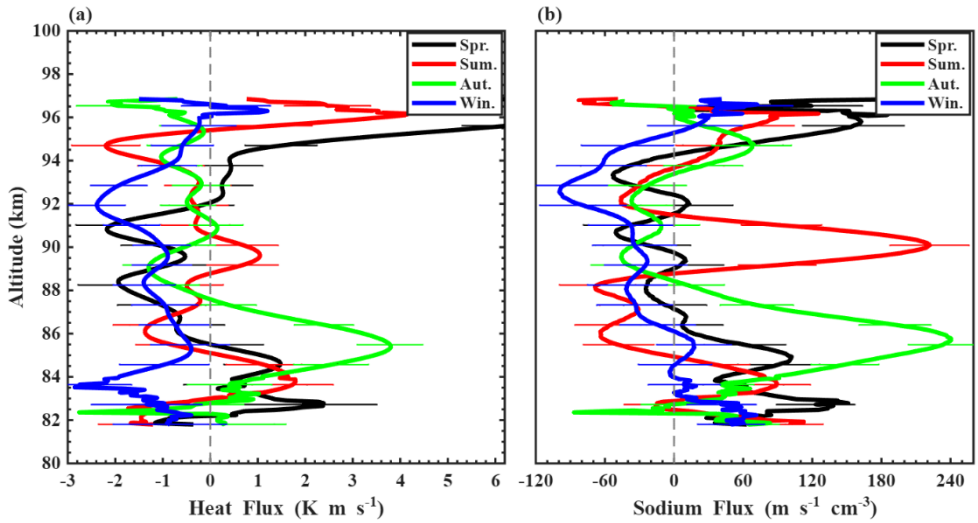

Figure 3. The seasonal profiles of the heat (a) and Na (b) fluxes. Spring (black), summer (red), autumn (green), winter (blue). Error bars are shown as thin lines.

Overall, the 3-minute temporal resolution is shown to retain the peak positions identified at the 30-minute resolution, while providing superior detail. This enhanced resolution successfully resolves atmospheric variations with periods of 5–6 minutes and longer.

Comment 2)

It would be helpful to the scientific community if the authors derive from their monthly mean Na, T, Na flux and heat flux profiles the annual and semi-annual fits and then compare them previous observations. For example, She et al. (2022) https://doi.org/10.1029/2021JD036291 have a nice Figure 1 which shows the annual and semi-annual amplitudes of fits to the T data from Ft. Collins, CO as well as how the mesopause height changes with season. Their Table 3 compares the seasonal temperature variations at several sites in both hemispheres, including at South Pole. How do the low-latitude Hainan data compare?

Response:

Thank you for your suggestion. Figure 4 presents the amplitudes of the annual, semi-annual, 4-month, and 3-month harmonic fits for the Hainan region. Due to the one-year dataset with observations primarily confined to winter, the fitting uncertainty increases for shorter periods; thus, we only consider the annual and semi-annual components

robust. For context, Table 1 compares the seasonal temperature variations at several sites in both hemispheres. The observed maximum amplitude of ~7 K at 85 km is closer to the 9.5 K value reported from Maui than to those of high-latitude stations, suggesting a potential signature of low-latitude mesopause dynamics.

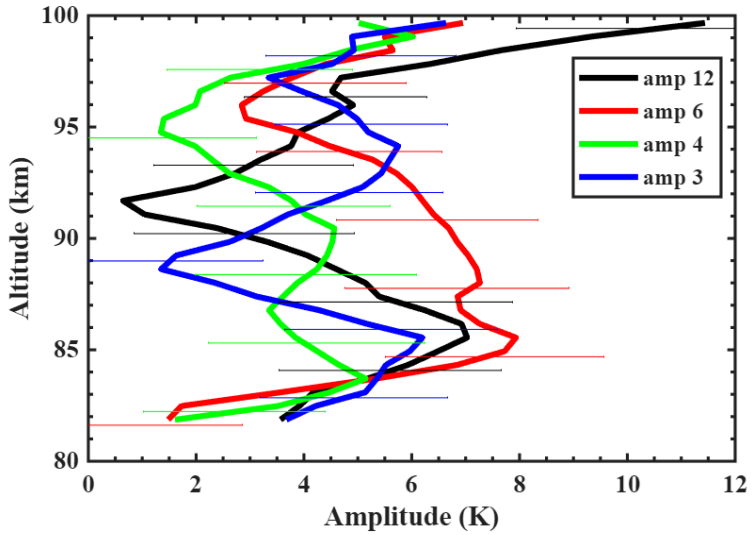

Figure 4. Seasonal harmonic amplitude profiles with the period of 12 (black), 6 (red), 4 (green), and 3 (blue) months. Error bars are shown as thin lines.

Table 1. Summary of Annual (12 months) Temperature Variations in the Mesopause Region

Site	References	Low-altitude maximum		High- altitude minimum	
		Altitude	12-month amplitude	Altitude	12-month amplitude
S Pole (90°S)	Pan and Gardner (2003)	85 km	32K	99 km	3.0K
Syowa (69°S)	Kawahara and Gardner (2004)	84 km	30K	98 km	5.0K
Kühlungsborn (54°N)	Gerding et al. (2008)	85 km	28K	102 km	3.0K
CSU (40.6°N)	She et al. (2022)	85.5 km	20K	98 km	1.0K
Urbana (40°N)	States and Gardner (2000)	85 km	14K	97.5 km	1.0K
Starfire (35°N)	Chu et al. (2005)	87 km	15K	96.5 km	1.0K
Maui (20.7°N)	Chu et al. (2005)	86 km	9.5K	97 km	3.5K
Hainan (19.5°N)	This manuscript	85.5 km	7K	92 km	0.7K

Comment 3)

Finally, Table 2 in the Hainan paper does not list the Na flux values from SOR and

Hefei. Why not? They were clearly provided in the referenced papers. And the data from McMurdo is not included (Chu et al., 2022, https://doi.org/10.1029/2021JD035728).

Response:

Thank you for pointing this out. To improve the rigor of the inter-station comparison, we have modified Table 2. Recognizing that the Na flux values for SOR, Hefei, and McMurdo were based on specific time periods rather than continuous annual data, we have added a dedicated "Observation Period" line. This addition provides essential context for the data and prevents the misinterpretation that all values are directly equivalent annual means. The table title has been updated accordingly to " Summary of Heat and Na Fluxes at Different Sodium Lidar Stations " to reflect this more precise and nuanced presentation.

Table 2. Summary of Heat and Na Fluxes at Different Sodium Lidar Stations

Stations	SOR New Mexico	Hefei, China	Maui, Hawaii	Hainan, China	Cerro Pachón, Chile	McMurdo, Antarctica
Latitude and longitude	35.0°N 106.5°W	31.5°N 117.2°E	20.7°N 156.3°W	19.5°N 109.1°E	30.3°S 70.7°W	77.84°S, 166.67°E
Observation period	Late Nov	Fall Mean	Annual Mean	Annual Mean	June	Late May
Resolutions (min)/ (km)	1.5/0.5	10/~3	1.5/0.96	3/~2	1/2	2.5/0.96
Heat flux peak (K m s^{-1})	−1.1	−1.04	−1.0	−0.8	−0.4	-3
Heat flux peak altitude (km)	~88	89–93	87–95	~89	~88	~84
Na flux peak (m $s^{-1}\cdot cm^{-3}$)	-225	-30	−80	−50	/	-55
Na flux peak altitude (km)	88	89-95	88	88–93	/	~84

References in this response:

1. She, C. Y., Yan, Z. A., Gardner, C. S., Krueger, D. A., & Hu, X. (2022). Climatology and seasonal variations of temperatures and gravity wave activities in the mesopause region above Ft. Collins, CO (40.6 N, 105.1 W). Journal of Geophysical Research: Atmospheres, 127(11), e2021JD036291. https://doi.org/10.1029/2021JD036291.
2. Chu, X., Gardner, C. S., Li, X., & Lin, C. Y. T. (2022). Vertical transport of sensible heat and meteoric Na by the complete temporal spectrum of gravity waves in the MLT above McMurdo (77.84 S, 166.67 E), Antarctica. Journal of Geophysical Research: Atmospheres, 127(16), e2021JD035728. https://doi.org/10.1029/2021JD035728.
3. Pan, W., & Gardner, C. S. (2003). Seasonal variations of the atmospheric temperature structure at South Pole. Journal of Geophysical Research, 108(D18), 4564. https://doi.org/10.1029/2002JD003217.
4. Kawahara, T. D., Gardner, C. S., & Nomura, A. (2004). Observed temperature structure of the atmosphere above Syowa Station, Antarctica (69S, 39E). Journal of Geophysical Research, 109, D12103. https://doi.org/10.1029/2003JD003918.
5. Gerding, M., Höffner, J., Lautenbach, J., Rauthe, M., & Lübken, F.-J. (2008). Seasonal variation of temperatures between 1 and 105 km altitude at 54 N by lidar. Atmospheric Chemistry and Physics, 8, 7465–7482. http://www.atmos-chem-phys.net/8/7465/2008/.
6. States, R. J., & Gardner, C. S. (2000). Thermal structure of the mesopause region (80–105 km) at 40oN latitude. Part I: Seasonal Variations. Journal of the Atmospheric Sciences, 57, 66–77. https://doi.org/10.1175/1520-0469(2000)057%3C0066:TSOTMR%3E2.0.CO;2.
7. Chu, X., Zhao, J., Lu, X., Harvey, V. L., Jones, R. M., Becker, E., et al. (2018). Lidar observations of stratospheric gravity waves from 2011 to 2015 at McMurdo (77.84°S, 166.69°E), Antarctica: 2. Potential energy densities, lognormal distributions, and seasonal variations. Journal of Geophysical Research: Atmospheres, 123, 7910–7934. https://doi.org/10.1029/2017JD027386.
8. Chu, X., Gardner, C. S., & Franke, S. J. (2005). Nocturnal thermal structure of the mesosphere and lower thermosphere region at Maui, Hawaii (20.7oN), and Starfire Optical Range, New Mexico (35oN). Journal of Geophysical Research, 110, D09S03. https://doi.org/10.1029/2004JD004891.
9. Li, T., Ban, C., Fang, X., Li, F., Cen, Y., Lai, D., Sun, C., Sun, L., Zhang, J., and Xu, C. (2022). Seasonal variation in gravity wave momentum and heat fluxes in the mesopause region observed by sodium lidar. Journal of Geophysical Research: Atmospheres, 127(23), e2022JD037558. https://doi.org/10.1029/2022JD037558.

Response to reviewer#2

Thank you for your careful works and valuable comments. The comments and suggestions are very useful for our manuscript. We have carefully studied these comments and suggestions and made some changes in our manuscript.

Comment 1)

In line 87, the photons should pass through a collimating lens, a narrow band optical filter and a converging lens, before being focused onto PMT.

Response:

Thank you for your comment. In response to feedback, we have revised the description of the optical path. Specifically, the order of components in the sentence has been corrected to: "The photons then pass through a collimating lens, a narrow band optical filter, and a converging lens before being focused onto the active area of a photomultiplier tube (PMT)." on page 4, line 87 of the manuscript.

Comment 2)

An improvement of the lidar shown in the manuscript is the frequency offset monitor unit. Was the measured frequency offset corrected in the lidar measurements shown in the Figure 6?

Response:

Thank you for your suggestion. Figure 6 displays the uncorrected vertical wind observations: the nightly average (solid line) and 30-minute profiles (dashed lines). The systematic offset in the average, as explained in Section 2.3, is attributed to the characterized laser frequency offset. Therefore, the corrected wind field, which essentially removes this known offset, is not separately plotted.

A comparison in Fig. 1 reveals consistent trends between the nightly-mean-subtracted vertical wind (black dashed line) and the frequency-offset-corrected wind (blue solid line), with the latter resolving finer atmospheric structures. This agreement supports the efficacy of the frequency monitoring module in correcting systematic instrumental biases.

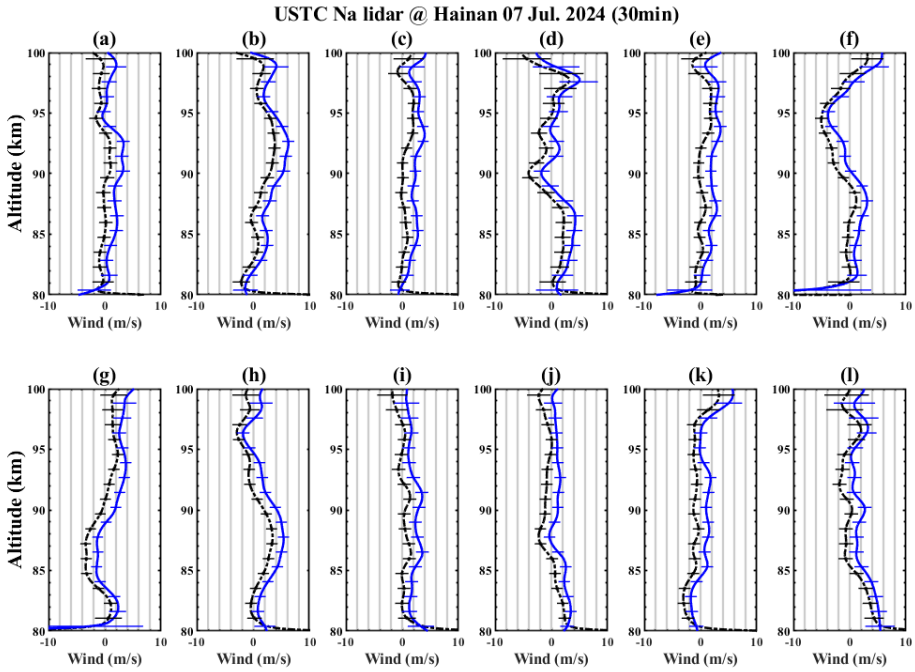

Figure 1. Sodium layer vertical wind (black dashed line) and the vertical wind after correcting frequency offset (blue solid line) at 30 minutes on 7 July 2024. Error bars are shown as thin lines.

Comment 3)

In the Figure8, the histogram color of the measurement hours is different from the color in the legend.

Response:

Thank you for pointing this out. When adjusting the color scheme of the figures to avoid red–green combinations, we inadvertently neglected to update the corresponding colors in the legends. This inconsistency has now been rectified, as illustrated in Fig. 2, and the same revision will be incorporated into the revised manuscript accordingly.

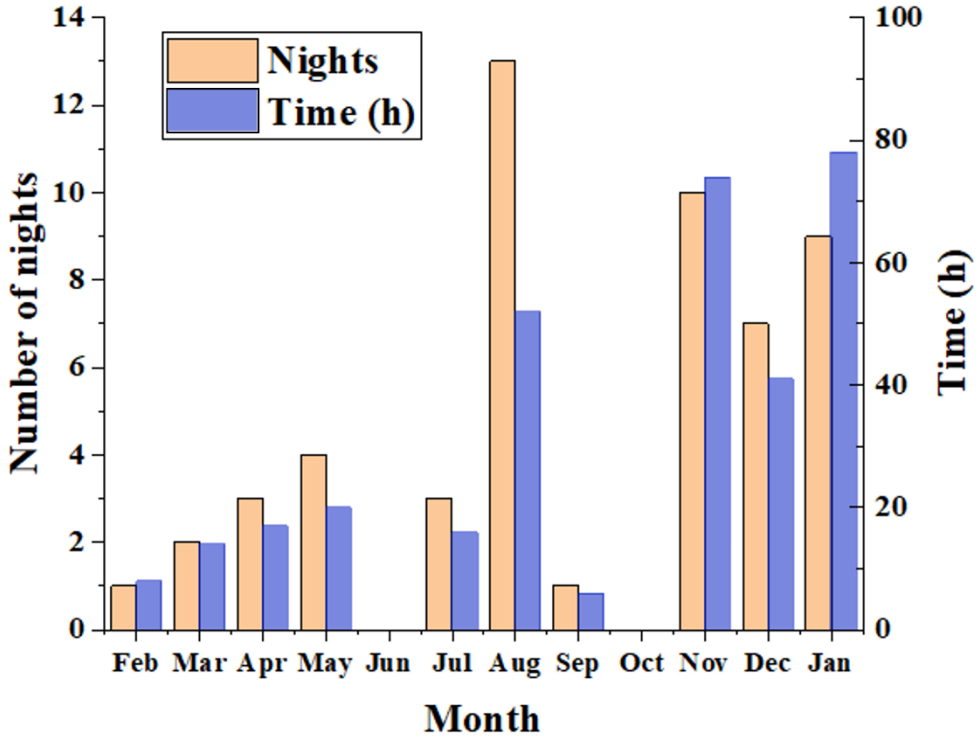

Figure 2. Histogram of number of nights and hours with valid data observed by the USTC sodium lidar at Hainan.